Journal of Materials Chemistry A

Accepted Manuscript

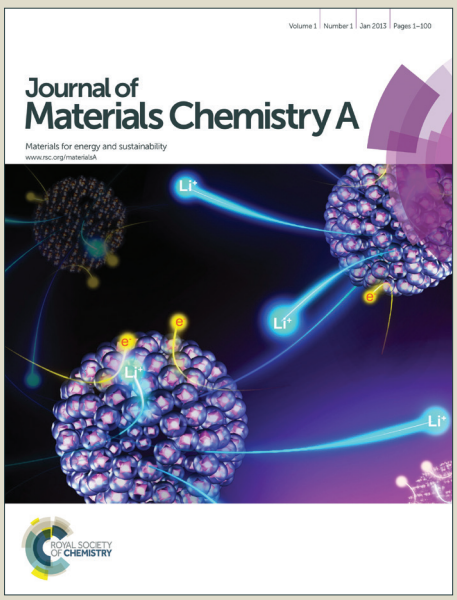

ROYAL SOCIETY OF CHEMISTRY

www.rsc.org/materialsA

Formation of Bilayer Clathrate Hydrates

Wen-Hui Zhao,[a,#] Jaeil Bai,[b,#] Lu Wang,[a] Lan-Feng Yuan,[*a] Jinlong Yang,[a] Joseph S. Francisco[b] and Xiao Cheng Zeng[*a,b]

[a]Hefei National Laboratory for Physical Sciences at Microscale, Department of Chemical Physics and Collaborative Innovation Center of Chemistry for Energy Materials, University of Science and Technology of China, Hefei, Anhui 230026, China

[b]Department of Chemistry, University of Nebraska-Lincoln, Lincoln, Nebraska 68588, USA

[*]Emails: *xzeng1@unl.edu; yuanlf@ustc.edu.cn*

[#]Both authors contribute equally to this work.

ABSTRACT:

We report molecular dynamics (MD) simulation evidence of a new family of two-dimensional (2D) clathrate hydrates. Particular attention is placed on the effect of size and hydrophilicity of guest-molecule on the formation of 2D clathrate hydrates. Among MD simulations undertaken, spontaneous formation of bilayer (BL) clathrate hydrates in nanoslits are found with five different hydrophobic guest molecules, namely, ethane (C_2H_6), ethene (C_2H_4), allene (C_3H_4), carbon dioxide (CO_2) and hydrogen (H_2) molecules, respectively. Our simulations suggest that the host cages in water framework are likely BL-hexagonal cages with single occupancy for H_2, or BL-heptagonal cages for CO_2. With further increase of guest size, the host cages for C_2H_6, C_2H_4, and C_3H_4 are BL-octagonal cages with single occupancy, and their long molecular axis tends to be normal to the surface of clathrate hydrates. In addition, for hydrophilic guest molecules such as NH_3 and H_2S which can form strong hydrogen bonds with water, we find that most guest molecules can preferentially displace water molecules from lattice sites of water framework, instead of being separately trapped within water cages. Structural analogy between the 2D and 3D clathrates enlightens us to predict stability of several bulk gas hydrates, namely, "ethane clathrate III", "CH_4 ice-*i*" and "H_2 ice-*i*". Our findings not only can enrich clathrate structures in the hydrate family but also may improve understanding of the hydrate formation in microporous media.

Introduction

Clathrate hydrates, ice-like crystalline compounds comprised of guest molecules trapped inside hydrogen-bonded water cages, can be formed spontaneously by cooling and/or compressing a mixture of guest molecules and water.[1] Understanding microscopic mechanism of clathrate hydrate formation has become an enduring research topics, not only because it belongs to the fundamental subjects of crystal growth from mixtures and self-ordering of water around guest molecules,[2] but also because it has important implications to energy resources, environment, chemical industries and geological hazard prevention.[3-9]

Over the past decade, considerable research efforts have been made to explore structures and physical properties of clathrate hydrates.[10-23] However, microscopic mechanism of the nucleation and growth of bulk clathrate hydrate is still not fully understood. This is due to the inability to precisely recording the time and spatial domain of a nucleation event on the experimental side, and also due to very long computing time required in typical molecular dynamics (MD) simulation of clathrate hydrate nucleation (a rare event) on the theoretical side.[21] Recently, several simulation studies have shown that low-dimensional clathrate gas hydrates, as well as guest-free hydrates, can be formed spontaneously on the time scale of nanoseconds in highly confined environment.[24-33] Moreover, the host cages formed in low-dimensional clathrate hydrates differ from those in bulk clathrate hydrates due to geometric constraints. The predicted low-dimensional clathrate hydrates not only enrich the gas hydrate family, but also open a door towards improved understanding of the hydrate formation in sediments or in porous media.

Previous experimental and theoretical studies indicate that the hydrate nucleation and growth are strongly dependent on the size of guest

molecules.[16,17] In this article, we perform systematic studies of the effect of guest-molecule size on the formation of two-dimensional (2D) gas hydrate (GH) by means of MD simulations. Our focus is on the bilayer (BL) clathrate hydrates formed in nanoslits with the guest molecules being ethane (C_2H_6), ethene (C_2H_4), allene (C_3H_4), carbon dioxide (CO_2), or the smallest hydrogen (H_2) molecules. In addition, formation of BL clathrate hydrates with the guest molecules being either NH_3 or H_2S molecules are examined as both guest molecules can entail strong H-bonding interaction with water molecules. We find that most hydrophilic guest molecules can preferentially displace water molecules from lattice sites of water framework, instead of being separately trapped within water cages. Based on these insights from the 2D simulations, we speculate a series of 3D stable clathrate structures.

Model and Methods

Classical MD calculations are performed to achieve spontaneous formation of the BL-clathrate hydrates when the binary fluid mixtures of water and guest molecules are confined in the nanoslit (width D = 0.8 nm to accommodate two layers of water[26]). The water molecule is described by the TIP5P model,[34] while TIP4P model is also examined for test simulations which give the same qualitative results of the bilayer hydrates formation as with the TIP5P model (see †Electronic Supplementary Information (ESI) for details). The OPLS potential models are chosen to simulate the C_2H_6, C_2H_4 and C_3H_4, NH_3 and H_2S molecules.[35,36] For proper electrostatic interaction representation, hydrogen molecule (H_2) is specifically modeled as a quadrupole with -0.64e charge at the center and +0.325e charge positioned at the two ends.[37] The CO_2 molecule is treated by EPM2 model.[38] A cutoff of 1.0 nm is used for interatomic interactions. Note that the cutoff method has been previously used to study the bilayer water.[32,33] Another widely used method for treating long-ranged electrostatic interactions in 2D structures is the slab-adapted Ewald sum method.[39] As summarized in a recent review,[29] both methods generally yield qualitatively the same bilayer ice

and bilayer methane hydrate structures, although the ferroelectric monolayer ice phases can be obtained by only using the slab-adapted Ewald sum method.[28,29] The guest molecules–wall and water-wall interactions are described by the 9-3 Lennard-Jones (LJ) potential function. The LJ and coulombic potential parameters are listed in ESI Table S1. All the MD simulations are performed using the GROMACS 4.5 package[40] with periodic boundary conditions in the lateral directions (i.e., x and y directions that are parallel to the confining walls). The z direction is normal to the confining walls. Temperature and pressure are controlled by the Nosé-Hoover thermostat[41] and Parrinello-Rahman barostat,[42] respectively.

Results and Discussion

In the first series of MD simulations, the simulation system consists of a binary fluid mixture of water and ethane molecules (with the H_2O/C_2H_6 ratio = 576:72=8:1, on the basis of test MD simulations). The lateral pressure (P_L) is set within the range of 200 MPa to 1 GPa to examine the pressure effect. The fluid system is initially equilibrated at a high temperature and then isobarically cooled in steps to a low temperature. Once the fluid system turns into a solid and reaches thermodynamic equilibrium at the low temperature, the temperature is raised again in steps. For all independent MD simulations with a different lateral pressure in the range of 200 MPa to 1 GPa, marked hysteresis-loop behavior for the internal energy versus temperature is seen (Figure 1), suggesting occurrence of a strong first-order phase transition for the confined binary mixture. Moreover, the inherent structure (obtained via applying the steepest-descent method to the final snapshot at the low temperature[30]) of the solid phase depends on the lateral pressure (see ESI Figure S1). For relatively low pressure (P_L = 200 MPa, Figure S1a), most ethane molecules congregate together within a cavity, behaving like a gas bubble, whereas other ethane molecules are separately encapsulated inside the BL octagonal water cages (with one ethane molecule per octagonal cage). These BL-octagonal water cages are part of a BL-amorphous ice which exhibits empty BL-pentagonal and BL-hexagonal cages, as well as a small

fraction of BL-heptagonal and BL-tetragonal cages.[30] With increasing pressure (P_L = 500 MPa, Figure S1b and P_L = 800 MPa, Figure S1c), more and more ethane molecules are involved in the formation of BL gas hydrates, *i.e.*, separately enclosed in the BL-octagonal cages. At the highest lateral pressure considered (P_L = 1 GPa), most ethane molecules are enclosed in the BL-octagonal cages (Figure S1d), while BL-tetragons connect the BL-octagonal cages (except some defects, *e.g.*, BL-pentagons), that is, a less perfect BL-octagon-tetragon hydrate is observed. Notably, double occupancy, *i.e.,* two ethane molecules being encapsulated in every single BL-decagonal cage, is also observed (Figure S1d). Still, phase-separated ethane gas bubbles exist in the BL clathrate hydrate. Also, importantly, the the MD trajectory (ESI Movie S1) show that the ethane molecules in "bubble" appear to be crystalline, which is different from bulk clathrate simulations where the guest molecule bubbles are fluid. Perhaps this behavior produces the kinetic barrier that hinders the formation of a perfect BL-clathrate.

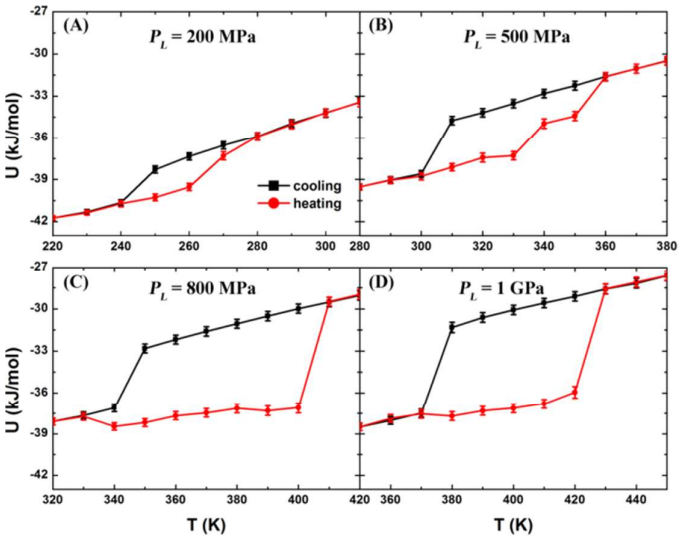

Figure 1. Temperature dependence of the potential energy U at various P_L for a mixture of water and ethane molecules confined in nanoslit.

When the solid hydrate is under heating, three kinds of behaviors have been observed at different lateral pressure: (1) for P_L = 200 MPa, the crystalline structure shows little change; (2) for P_L = 800 MPa or 1 GPa, increasing number of ethane molecules are separately enclosed in the BL-octagonal cages, corresponding to the dip

in potential-energy curves (Figures 1C and D, 330-340 K and 370-380 K, respectively); (3) for P_L = 500 MPa, when the system is heated up to 340 K, coexisting liquid-water/ethane-bubble/BL-clathrate can be observed, which remains unchanged at 350 K. This result corresponds to the potential energy step at temperature range of 340-350 K for P_L = 500 MPa (Figure 1B).

On basis of the inherent structures shown in Figure S1 and the structure features of the BL-octagon-tetragon ethane hydrate (the details will be discussed below), every ethane molecule encaged in BL-octagonal cages is perpendicular to the confining walls, *i.e.*, parallel to the *z* axis. To characterize the degree of nucleation and growth for the BL-clathrate, an order parameter *S* is defined as:

$$\boldsymbol{S = \frac{1}{2N}\sum_{i}^{N_A}(3cos^2\theta_i - 1)}, \qquad (1)$$

where θ_i is the angle between the long molecular axis of the *i*-th ethane molecule and the *z* axis, N_A is the number of isolated ethane molecules encapsulated in water cage (Here the isolated ethane molecule is defined such that any ethane molecule that is entirely surrounded by water molecules, *i.e.*, the ethane molecule is enclosed inside the BL-water cage), and *N* is the total number of ethane molecules. The summation over N_A in Eq. (1) means that ethane molecules involved in ethane bubbles are excluded from the summation. As such, the order parameter *S* is 1 for the perfect BL-clathrate structure and 0 for phase-separated liquid.

Figure 2 shows time-dependent potential energy *U* and order parameter *S* for typical nucleation and growth of BL-clathrate hydrate (see Movie S1) at 370 K and 1 GPa, starting from a phase-separated liquid water with an ethane bubble (pre-equilibrated at 380 K and 1 GPa; Figure 2A). In the first several nanoseconds, stochastic nucleation events of ethane-containing BL-octagonal cages arise. At ~7.5 ns, a clear jump in *S* from zero to ~0.2 and a small drop in U (by ~1 kJ/mol) can be seen, indicating post-nucleation process (Figure 2B). Beyond 75 ns, with more and more ethane molecules being separately incorporated into BL octagonal cages

(Figures 2C and D), marked growth of ethane hydrate is observed, as indicated by the precipitous rise of *S* and fall of U. At ~200 ns, a small domain of ethane bubble is enclosed in the hydrate (Figure 2E), hindering further growth of the hydrate. Some BL-pentagonal "defects" formed to connect the BL-octagonal cages result in a less perfect BL-clathrate hydrate (Figure 2F).

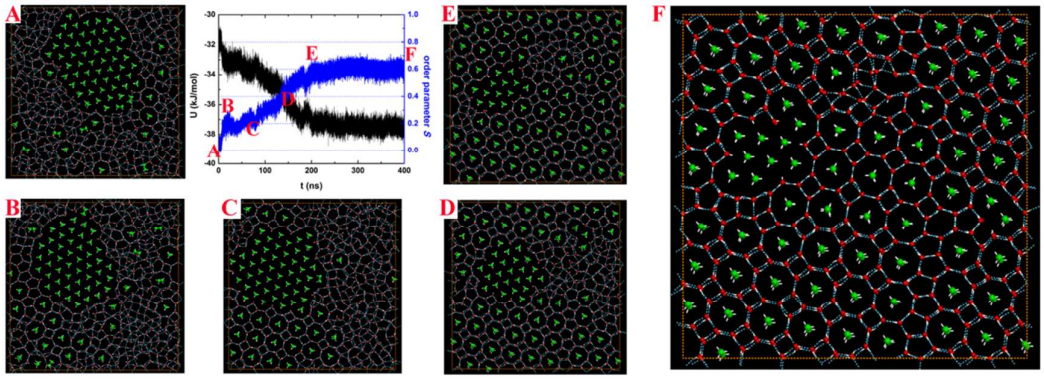

Figure 2. Time-dependent potential energy *U* (black curve) and order parameter *S* (blue curve) for the confined ethane-water system during the course of nucleation and growth of the BL-clathrate hydrate at T = 370 K and P_L = 1 GPa. Snapshots (A) through (F) display structural evolution at different time-stage of MD simulation marked in the time-dependent *S* curve. Color code: O, red; H, white; C, green; hydrogen bond, blue dotted line.

To remove the ethane bubble and the BL-pentagonal "defects", we design a thermodynamic path in the MD simulation to achieve a near-perfect BL-ethane hydrate crystal, including the cyclic heating/annealing, stepwise compression, and long-time incubation. Starting from a three-phase coexistence structure as shown in Fig. 3A, which is obtained at 350 K on heating and at 500 MPa, the lateral pressure of the system is increased to 600 MPa for 20 ns and then to 700 MPa for 100 ns. Next, the temperature and lateral pressure of the system are raised instantly to 360 K and 800 MPa for 50 ns. The MD trajectory (Movie S2) and order parameters *S* (Figure S2) demonstrate that the octagon-square domain grows gradually. Furthermore, the temperature and pressure of the system are increased instantly to 390 K and 1 GPa and kept for 200 ns (Movie S3). Most ethane molecules are separately encapsulated in BL-octagonal cages, which are connected by BL-tetragons (Fig. 3B). Lastly, we

perform a simulation for 160 ns at 430 K and 1.5 GPa to produce a perfect BL-clathrate hydrate (as shown in Fig. 3C and Movie S4). Note that the perfect BL-clathrate order parameter S ~ 0.8 is less than 1 (Fig. S2), suggesting the ethane axis tilting with z axis because of thermal motions. As temperature decreases, majority of ethane molecules in the hydrate are aligned vertically (Fig. S3). And the inherent structures show that ethane molecules are normal to the confining wall due to absence of thermal motions. It can also been seen from Fig. 3B that some water molecules are separately enclosed in water cages (blue marked), *i.e.* interstitial water, indicating the transformation among the water cages through water pair insertions/removals and rotations. Similar behavior was observed from MD simulation of bulk hydrate growth,[22] and these interstitial water molecules may facilitate the growth of hydrate crystals.

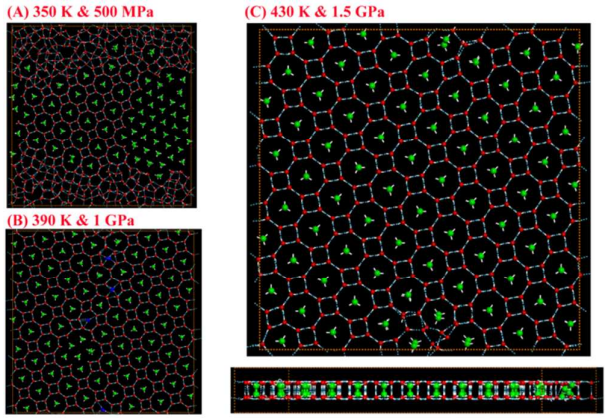

Figure 3. A designed thermodynamic path in the MD simulation to grow a nearly-perfect BL ethane clathrate crystal. (A) A three-phase coexistence structure at 350 K and 500 MPa. (B) A less perfect BL-clathrate hydrate at 390 K and 1 GPa. (C) Top and side views of the inherent structure of a perfect BL-clathrate hydrate at 430 K and 1.5 GPa. The blue spheres in (B) represent the water molecules separately enclosed in water cages, *i.e.* interstitial water.

Both Figures 2 and 3 demonstrate that crystallization of the BL ethane clathrate proceeds *via* a multistep nucleation and growth. First, most ethane molecules gather together and form a dense bubble. The ethane bubble persists in solution, and at the nucleation stage, the ethane molecules at the edge of bubble or those dissolved in solution are trapped in BL-octagonal cages to form clathrate nuclei. However, these

early BL-octagonal cages can easily collapse before becoming critical nuclei, which consists of at least four octagons according to observation of MD trajectories. Second, those nuclei larger in size than the critical nucleus grow and some BL-polygon "defects" (BL-pentagons in particular) are formed within the solid nuclei, resulting in a seed of amorphous clathrate. Note that the bubble and BL-pentagonal defects can block the formation of a perfect BL-clathrate. As shown in Figure 3C, starting from the three-phase coexistence, upon cyclic heating/annealing, stepwise compression, and long-time incubation, the BL amorphous clathrate develops into a nearly-perfect BL-clathrate crystal. This multistep nucleation mechanism is consistent with the two-step nucleation mechanism revealed in bulk clathrates.[15-18, 21-23]

To gain more insight into the structural features of BL-octagon-tetragon ethane hydrate, we examine the lateral site-site radial distribution functions (RDFs) and the transverse density profiles of phase-separated liquid at 1 GPa and 450 K and a perfect BL-clathrate, as shown in Fig. 4 and Fig. 5. The oxygen (O)-oxygen (O) RDF (g_{OO}^{xy}) of liquid exhibits typical liquid behavior, including a pre-peak representing a bilayer liquid, and a prominent first peak at r_{xy} ~ 0.28 nm, followed by decaying peaks, and eventually approaching to unity indicating a disordered state, while g_{OO}^{xy} of the clathrate hydrate shows features of sharp peaks owing to the long-range order: the first peak (at r_{xy} ~ 0) corresponds to the solid bilayer and the hydrogen bonding between two monolayer water (normal to the walls); and the second peak (at r_{xy} ~ 0.27 nm) indicates the in-plane hydrogen bonds. Moreover, the methyl (C)-methyl (C) RDF (g_{CC}^{xy}) for phase-separated liquid also shows sharp peaks. However, this does not mean the long-range order but a high-density ethane bubble, which can be also seen from the methyl (C)-oxygen (O) RDF (g_{CO}^{xy}) in that the first peak of liquid is very low (< 1). The first and second peaks of g_{CC}^{xy} for phase-separated liquid suggest that some ethane molecules are oriented normal to the walls (at r_{xy} ~ 0) and some are parallel to the walls (at r_{xy} ~ 0.15 nm). On the other hand, g_{CC}^{xy} of clathrate hydrate exhibits long-range order, and the first peak indicates the ethane molecules are normal to the walls (at r_{xy} ~ 0), and the second peak (at r_{xy} ~ 0.65 nm) corresponds to the

lateral distance between the center of nearest-neighbor octagons, while the third peak (at r_{xy} ~0.92) corresponds to the lateral distance between the center of second nearest-neighbor octagons (connected by tetragons). The disappearance of the peak at r_{xy} ~ 0.15 nm suggests that all ethane molecules are normal to the walls. The first peak of g_{CO}^{xy} for clathrate hydrate corresponds to the "radius" of octagons (the lateral distance between ethane molecules and their nearest-neighbor waters which form the octagons).

Figure 5 shows computed transverse density profiles of oxygen, hydrogen and ethane (methyl, CH_3) in the *z*-direction (normal to the confining walls). The distribution of oxygen for the BL-clathrate hydrate exhibits two sharp peaks, suggesting a solid state, whereas that for the phase-separated liquid is broad. The distribution of hydrogen atoms in the BL-clathrate hydrate exhibits four sharp peaks, two close the peaks of oxygen, indicating that the OH bond is parallel to the confining walls, and another two at the distance of 0.1 nm from the peak of oxygen, indicating that the OH bond is normal to the confining walls. Amplitude of the peaks of hydrogen that are parallel to the confining walls is about three times higher than that normal to the confining walls, indicating that among the four water molecules in one tetragon, two are parallel to the confining walls, and another two are normal to the confining walls. The distribution of methyl (CH_3) in the phase-separated liquid is also broad, while that for the BL-clathrate hydrate exhibits two sharp peaks with a distance of 0.15 nm, close to C-C bond length of ethane molecule and suggesting the ethane molecule in BL-clathrate hydrate is normal to the confining walls.

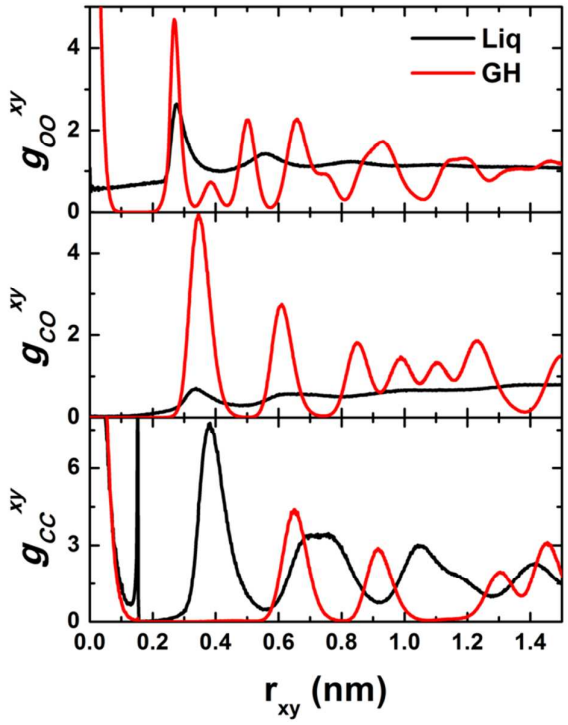

Figure 4. Computed lateral site-site radial distribution functions (RDFs) g(r_{xy}) for phase-separated liquid (Liq) and bilayer-gas hydrate (GH).

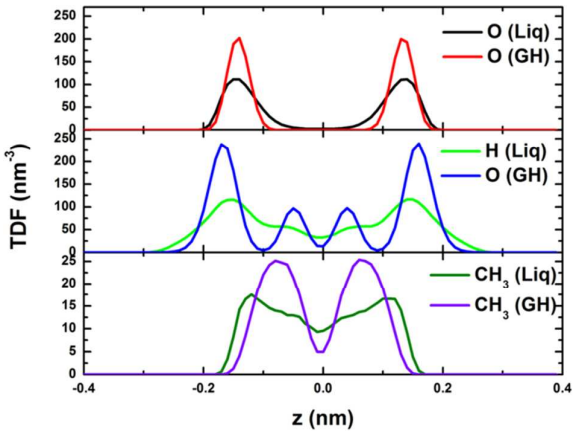

Figure 5. Transverse density profiles for phase-separated liquid and gas hydrate.

From Figure 3C, one can see that the water framework of BL ethane clathrate is identical to that of BL methane clathrate,[26] *i.e.*, the Archimedean $4{\cdot}8^2$ (square-octagon) pattern, even though an ethane molecule has a longer molecular axis than that of CH_4. Actually, if the long molecular axis of ethane is normal to the surface of the clathrate hydrate, the lateral size of ethane is comparable to that of CH_4. Hence both molecules

can give rise to the same water framework. To further test this conjecture, we also perform several independent simulations for binary fluid mixtures of water/ethene and water/allene. All of these molecules have similar lateral size, while the perpendicular length of allene is longer than that of ethane. It turns out that ethene and allene can also form nearly-perfect clathrate hydrates, and their water frameworks also exhibit the Archimedean $4{\cdot}8^2$ (square-octagon) pattern (see Figures S4-S6), and the molecular axis of both ethene and allene molecules is also normal to the plane of BL-clathrate hydrates. Also, importantly, stabilities of the BL-square-octagon clathrates for the three linear molecules are confirmed by ab initio computation (see ESI for details).

Thus far, we have shown that the three linear molecules can lead to the same water framework as CH_4 guest. How about guest molecules smaller than CH_4? To address this question, we perform another series of independent MD simulations to seek BL CO_2 and H_2 hydrates from two kinds of initial configurations. First, we construct a perfect BL-clathrate hydrate ($4{\cdot}8^2$ pattern) with either CO_2 or H_2 molecules replacing the ethane molecules. We then start the MD simulation (in the *NVT* ensemble) with the BL-hydrate for CO_2 (H_2) as the initial structure and at 100 K, followed by stepwise raise of temperature towards 300 K. For the CO_2 hydrate, the BL-octagonal cages start to collapse when the temperature reaches 240 K. Eventually, most BL-octagonal cages are transformed to BL-heptagonal cages connected by BL-pentagons (Movie S5).

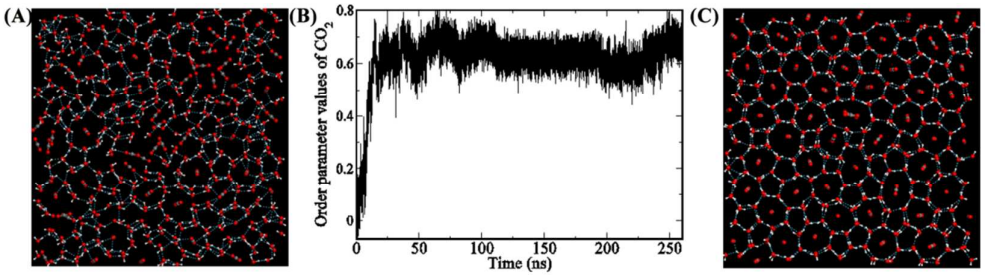

Figure 6. (A) A snapshot of mixed gas and hydrate at 300 K and 1 GPa. (B) Time-dependent *S* during system equilibration at 325 K and 1.5 GPa for 260 ns. As more CO_2 dissolved into bilayer water, more CO_2 are aligned normal to the surface of clathrate. (C) A snapshot of hydrate structure at 260 ns, which is amorphous-like. Most CO_2 molecules are located within BL-heptagonal cages while a small number of them are trapped inside BL-octagonal cages. Color code: O, red; H, white; C, grey.

Another MD simulation is started from a binary fluid mixture of water and CO_2 (see Figure 6). Specifically, a mixture of 50 CO_2 and 400 water molecules is equilibrated at 800 K and 1 GPa, followed by an instant cooling to 250 K. After 20 ns equilibration, a mixture of gas and hydrate is formed where some CO_2 molecules are separately enclosed in BL-octagonal or BL-heptagonal cages, while many CO_2 molecules are not dissolved into water. To render more CO_2 molecules dissolved into water, the gas and hydrate mixture is heated to 300 K and compressed at 1 GPa for 40ns (Figure 6A). Next, the system is equilibrated at 325 K and 1.5 GPa for 260 ns (Figure 6B) from which an amorphous-like BL CO_2 hydrate structure is formed (see Figure 6C). Since CO_2 molecules can be separately encapsulated in either heptagonal or octagonal cages (Figure 6C), some CO_2 molecules are aligned in horizontal direction at low temperature. Figure S7A shows CO_2 molecular orientation versus temperature with respect to the z direction (surface normal of the clathrate) in the BL-amorphous hydrate. As temperature decreases, majority of CO_2 in the hydrate are aligned in the z direction (θ being ~16 degree), while others are aligned horizontally (θ being ~90 degree) below 50 K. Figure S7B shows that the order parameter S of CO_2 increases as temperature decreases.

Next, starting with a constructed H_2 hydrate, similar *NVT* MD simulation shows that the BL-octagonal cages collapse at 150 K, indicating that the H_2 BL-clathrate with $4{\cdot}8^2$ pattern is mechanically unstable even at very low temperature. Another MD simulation starts with a binary fluid mixture of water and H_2 (with 20% mole fraction of H_2) at 300 K and 1 GPa, and it leads to a BL amorphous hydrate (Figure 7A). In this amorphous structure, there are not only BL-hexagonal cages occupied by single H_2, but also BL-heptagonal cages accommodating two H_2 molecules (*i.e.*, double occupancy), and even BL-octagonal cages that encaging three H_2 molecules, and BL-nonagonal cages encapsulating four H_2 molecules. Note that the water framework of BL amorphous hydrate is identical to the BL-amorphous ice.[30] We know that the BL-amorphous ice is a metastable phase, whereas the BL-hexagonal ice is the thermodynamically stable phase since the latter can be obtained by annealing the

former through repeated cycles of cooling and heating.[26,31] Thus, we speculate that a possible ideal BL H_2 clathrate could be a BL-hexagonal crystal with single occupancy of H_2 in each hexagonal cage (Figure 7B). To verify this speculation, we examine thermal stability of such a BL-hexagon H_2 clathrate crystal *via* an MD simulation in *NVT* ensemble for temperature changing from 100 to 300 K. For $T \leq 270$ K, the constructed BL-hexagonal H_2 clathrate does not show signs of decomposition or cage collapse. At 280 K, the cages start to collapse (Movie S6). Stability of the BL-hexagonal H_2 clathrate is also confirmed by ab initio computation (see ESI for details). The thermodynamic path to achieve the near-perfect BL-hexagonal H_2 clathrate will be undertaken in future.

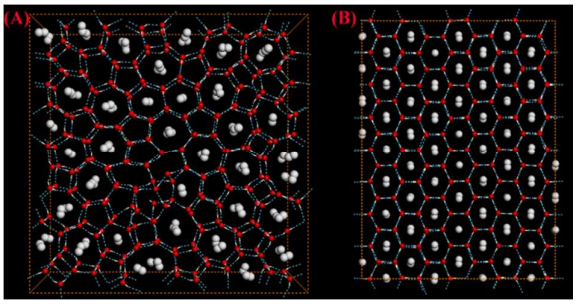

Figure 7. (A) A snapshot of a BL amorphous H_2 clathrate. (B) A constructed perfect BL-hexagonal H_2 clathrate. Red spheres represent oxygen, white small spheres hydrogen of water, white big spheres hydrogen molecules, and blue dotted lines hydrogen bonds.

As a summary, for the smallest diatomic molecule H_2, the host cage is likely BL-hexagon for single occupancy, BL-heptagon for double occupancy, BL-octagon for triple occupancy, and BL-nonagon for quadruple occupancy. For CO_2 with size being between that of H_2 and CH_4, the host cage is likely BL-heptagon for single occupancy. With further increase of molecular size, for CH_4[26] and linear molecules with similar lateral size, such as C_2H_6, C_2H_4, and C_3H_4, the host cage is BL-octagon with single occupancy. The long molecular axis of the latter three molecules tends to be normal to the surface of clathrate hydrates.

Thus far, all the guest molecules we have considered are hydrophobic. It is commonly believed that highly hydrophilic molecules cannot serve as guest molecules as they tend to disrupt hydrogen-bonding networks, however, there are indeed evidences from experiments and MD simulations of stable clathrates with some guests forming strong hydrogen bonds with water.[43-47] Can these hydrophilic molecules support stable BL-clathrates as well? To explore this possibility, we first examine stability of a constructed BL-clathrate NH_3 hydrate with the $4{\cdot}8^2$ pattern since NH_3 is comparable to CH_4 in size. Based on MD simulations (in the *NVT* ensemble) with temperature increasing in steps from 100 to 300 K, we see signs of cage collapse at 180 K (Movie S7). Alternatively, we examine possibility of spontaneous formation of BL NH_3 hydrate by starting MD simulation (in the NP_LT ensemble with the ratio of H_2O/NH_3 = 576/72=8/1) from a high temperature fluid (equilibrated at 1000 K and 1 GPa), followed by an instant quench to 250 K. After 100 ns, the obtained hydrate structure resembles that of the BL-rhombic ice[48] except that some water molecules are displaced by NH_3 molecules from lattice sites of rhombic structure (Figure 8A, and Movie S8).

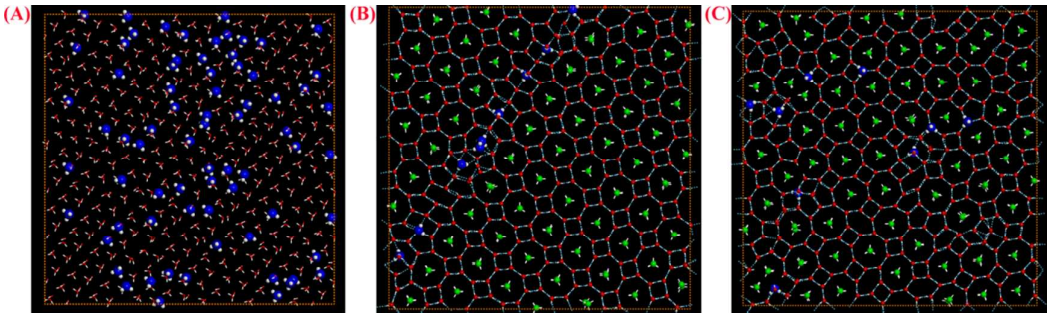

Figure 8. (A) The inherent structure of BL mixture of water and NH_3. (B) A snapshot structure obtained *via* heating the "perfect" binary C_2H_6 and NH_3 hydrate to 300 K. (C) The final snapshot obtained from the simulation (starting from a fluid mixture, and the system is instantly cooled to 250 K at fixed lateral pressure, and then heated again to 260 K and to 270 K). Color code: O, red; H, white; N, blue; C, green; hydrogen bond, blue dotted line.

We note a recent simulation and experimental study shows that the addition of methane molecules can stabilize the very unstable NH_3 clathrate, although the mixed

clathrate is still far less stable that the pure methane clathrate.[47] Enlightened by this study, we examine stability of a perfect BL-ethane hydrate with the $4{\cdot}8^2$ pattern and with a portion of guests replaced by NH_3 molecules. Although the main water framework consisting of the cages containing C_2H_6 remains stable at 300 K, the cages containing NH_3 starts to collapse even at 160 K, and the NH_3 and water molecules form BL-polygons (Figure 8B and Movie S9). The collapse of the NH_3 cages suggests that the hydrophilic molecules (such as NH_3) can destabilize the clathrate structure.

We also examine possibility of the formation of binary C_2H_6 and NH_3 hydrate by cooling a fluid mixture of C_2H_6, NH_3 and water (with the ratio of $H_2O/C_2H_6/NH_3$ = 576/63/9=64/7/1). Remarkably, a mixed clathrate is eventually formed (see Figure 8C). Here, the BL water frame structure (besides some BL-polygon defects) is identical to that of BL-ethane clathrate, *i.e.*, $4{\cdot}8^2$ pattern. The ethane molecules are separately encapsulated in BL-octagonal cages, while NH_3 molecules preferentially displace some water molecules from lattice sites (Movie S10). NH_3 molecules in cages are also observed. Also, interestingly, the MD trajectory shows that the NH_3 molecules diffuse about much more rapidly while the hydrophobic guests and their surrounding water molecules stay in place (Movies S8-S10). The rapid diffusion of NH_3 molecules may be the reason of the destabilization of NH_3 clathrate. Interestingly, for another hydrophilic molecule, *i.e.*, H_2S molecule, similar behaviors are also observed from the MD simulations of BL-H_2S hydrate (see Figure S8 and Movie S11).

Additional Remarks on Connection with 3D Methane Hydrates

(1) We have demonstrated the formation of 2D BL-clathrate ethane, ethene or allene hydrates where the guest molecules preferred to be entrapped inside BL-octagonal cages. Are there any structural analogy between the 2D and 3D (bulk) ethane clathrates? In other words, can these linear molecules be separately entrapped in "octagonal" cages in bulk clathrates? One hint can be gained from structures of the high-pressure methane and argon hydrate III phases[49,50] since in these bulk hydrates,

typical 2D plane is composed of tetragons and octagons. Motivated by this hint, we perform a test MD simulation and confirm that indeed the methane hydrate III can be stable at room temperature and 3 GPa (Figure S9). Next, we construct a new "ethane clathrate III" whose water framework resembles that of the methane hydrate III. Here, ethane molecules are separately enclosed in octagonal cages. The "ethane clathrate III" is first optimized at zero temperature with a fixed volume. Then the system is heated at several different pressures. Our MD simulation shows that the "ethane clathrate III" is stable at 3 GPa with temperature below 320 K (Figure 9A).

(2) Another hint can be gained from the "ice-*i*", which is a stable guest-free ice clathrate observed only in computer simulations.[51] We construct a new methane clathrate (CH_4 ice-*i*) in which the methane molecules are separately entrapped by "octagonal cages" (see Figure 9B). The new solid hydrate is heated stepwise at a fixed pressure (200 MPa). The melting temperature of "CH_4 ice-*i*" is about 240 K, close to that of guest-free bulk ice clathrate (ice-*i* melts at 250 K and 200 MPa).[51] We have also examined stability of "ethane ice-*i*" and find that the hand-made hydrate cannot be stable even at 0 K. However, when the Lennard-Jones parameters of CH_3 are reduced to those of hydrogen (*i.e.*, σ = 0.266 nm and ε = 0.125 kJ/mol) while keeping the bond length (CH_3-CH_3) unchanged, the "ethane ice-*i*" can be stable, suggesting that "hydrogen ice-*i*" may be a stable hydrate. Examination of the stability of the bulk "hydrogen ice-*i*" using first-principles method will be undertaken in future.

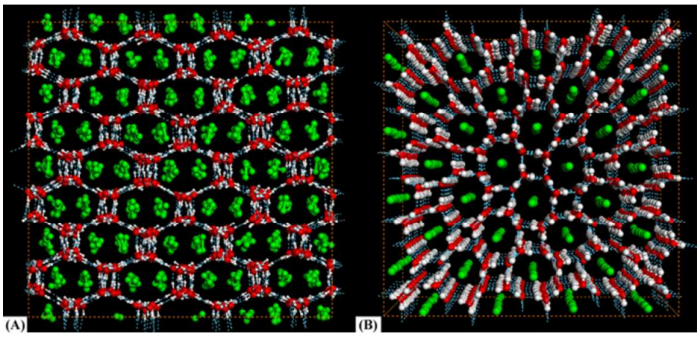

Figure 9. Snapshots of (A) the constructed "ethane clathrate III" at 3 GPa and 300 K and (B) constructed "CH_4 ice-*i*" at 200 MPa and 230 K.

Conclusions

Based on numerous MD simulations, a number of stable BL crystalline and amorphous gas hydrates with either hydrophobic or hydrophilic guest molecules are obtained within a nanoslit. Our MD results demonstrate that the host water cages depend on the size of guest. For example, for the smallest diatomic molecule H_2, despite of amorphous structure observed, the BL-hexagonal clathrate is mechanically most stable for single occupancy of H_2 molecule per cage. For a larger guest molecule CO_2, the amorphous clathrate entails mostly the BL-heptagonal cages with single occupancy of CO_2 molecule per cage. For several molecules with size larger than CO_2, *i.e.*, CH_4,[26] or linear molecules C_2H_6, C_2H_4, and C_3H_4, the BL-square-octagonal clathrate structure is formed, where the three linear molecules can be accommodated within the BL-octagonal cages by adjusting their molecular orientation. This adjustment of molecular orientation of linear molecules may be a reason that seemingly different guests can be enclosed in the same type of water cage in bulk clathrate hydrate.

In addition, for hydrophilic guest molecules such as NH_3 and H_2S which can form strong hydrogen bonds with water, most guest molecules can preferentially displace water molecules, one for each, from lattice sites of water framework rather than being separately trapped within water cages. Furthermore, for the mixture of C_2H_6 and NH_3, a mixed clathrate identical to BL-ethane clathrate, in which the ethane molecules are separately encapsulated in BL-octagonal cages and NH_3 molecules preferentially displace some water molecules from lattice sites, is observed. Our simulations also show that the NH_3 molecules diffuse about much more rapidly while the hydrophobic guests and their surrounding water molecules stay in place. The rapid diffusion of NH_3 may be the reason of the destabilization of clathrate.

Finally, structural analogy between the 2D and 3D (bulk) ethane clathrates is analyzed. Motivated from the unique feature of "BL-octagonal cages" in many 2D

clathrate hydrates, we have predicted stability of bulk "ethane clathrate III", "CH_4 ice-*i*" and "H_2 ice -*i*". These newly predicted bulk clathrate hydrates as well as their structural similarity with 2D BL clathrate hydrates call for future experimental confirmation.

Acknowledgements

This work is supported by MOST (2011CB921400), by NSFC (21121003, 2123307), by the Fundamental Research Funds for the Central Universities (WK2060030012), by CAS (XDB01020300, XDB10030402). XCZ is supported by grants from University of Nebraska Center for Energy Sciences Research, and a grant from USTC for (1000plan) Qianren-B summer research. WHZ and XCZ are also supported by a grant (1401042004) from Bureau of Science & Technology of Anhui Province.

Notes and references

[†]Electronic supplementary information (ESI) available: Figures S1-S9, Table S1, independent MD simulations with TIP4P water model, the density-functional theory structural optimizations, and Movies S1-S11.

1 E. D. Sloan and C. A. Koh, *Clathrate Hydrates of Natural Gases*, CRC Press, Boca Raton, FL, 3rd edn, 2008.

2 J. Vatamanu and P. G. Kusalik, *J. Phys. Chem. B* 2006, **110**, 15896-15904.

3 E. D. Sloan, *Nature* 2003, **426**, 353-359.

4 L. J. Florusse, C. J. Peters, J. Schoonman, K. C. Hester, C. A. Koh, S. F. Dec, K. N. Marsh and E. D. Sloan, *Science* 2004, **306**, 469-471.

5 W. L. Mao, H.-k. Mao, A. F. Goncharov, V. V. Struzhkin, Q. Guo, J. Hu, J. Shu, R. J. Hemley, M. Somayazulu and Y. Zhao, *Science* 2002, **297**, 2247-2249.

6 Y. Park, D.-Y. Kim, J.-W. Lee, D.-G. Huh, K.-P. Park, J. Lee and H. Lee, *Proc. Natl. Acad. Sci. U.S.A.* 2006, **103**, 12690-12694.

7 K. Kaiho, T. Arinobu, R. Ishiwatari, H. E. G. Morgans, H. Okada, N. Takeda, K. Tazaki, G. Zhou, Y. Kajiwara, R. Matsumoto, A. Hirai, N. Niitsuma and H. Wada, *Paleoceanography* 1996, **11**, 447-465.

8 C. R. Fisher, I. R. MacDonald, R. Sassen, C. M. Young, S. A. Macko, S. Hourdez, R. S. Carney, S. Joye and E. McMullin, *Naturwissenschaften* 2000, **87**, 184-187.

9 D. J. Milton, *Science* 1974, **183**, 654-656.

10 D. K. Staykova, W. F. Kuhs, A. N. Salamatin and T. Hansen, *J. Phys. Chem. B* 2003, **107**, 10299–10311.

11 A. Klapproth, E. Goreshnik, D. Staykova, H. Klein and W. F. Kuhs, *Can. J. Phys.*, 2003, **81**, 503–518.

12 J. M. Schicks and J. A. Ripmeester, *Angew. Chem., Int. Ed.*, 2004, **43**, 3310–3313.

13 M. M. Murshed and W. F. Kuhs, *J. Phys. Chem. B* 2009, **113**, 5172–5180.

14 H. Ohno, T. A. Strobel, S. F. Dec, E. D. Jr. Sloan and C. A. Koh, *J. Phys. Chem. A* 2009, **113**, 1711–1716.

15 L. C. Jacobson, W. Hujo and V. Molinero, *J. Am. Chem. Soc.*, 2010, **132**, 11806–11811.

16 L. C. Jacobson, W. Hujo and V. Molinero, *J. Phys. Chem. B* 2010, **114**, 13796–13807.

17 J. S. Loveday and R. J. Nelmes, *Phys. Chem. Chem. Phys.* 2008, **10**, 937-950.

18 J. Vatamanu and P. G. Kusalik, *Phys. Chem. Chem. Phys.*, 2010, **12**, 15065–15072.

19 L. C. Jacobson and V. Molinero, *J. Am. Chem. Soc.*, 2011, **133**, 6458–6463.

20 G.-J. Guo, Y.-G. Zhang, C.-J. Liu and K.-H. Li, *Phys. Chem. Chem. Phys.,* 2011, **13**, 12048–12057.

21 M. R. Walsh, C. A. Koh, E. D. Sloan, A. K. Sum and D. T. Wu, *Science*, 2009, **326**, 1095–1098.

22 M. R. Walsh, J. D. Rainey, P. G. Lafond, D.-H. Park, G. T. Beckham, M. D. Jones, K.-H. Lee, C. A. Koh, E. D. Sloan, D. T. Wu and A. K. Sum, *Phys. Chem. Chem. Phys.*, 2011, **13**, 19951-19959.

23 M. R. Walsh, G. T. Beckham, C. A. Koh, E. D. Sloan, D. T. Wu and A. K. Sum, *J. Phys. Chem. C* 2011, **115**, 21241-21248.

24 H. Tanaka and K. Koga, *J. Chem. Phys.* 2005, **123**, 094706.

25 J. Bai, C. A. Angell and X. C. Zeng, *Proc. Natl. Acad. Sci. U.S.A.* 2010, **107**, 5718 – 5722.

26 J. Bai and X. C. Zeng, *Proc. Natl. Acad. Sci. U.S.A.* 2012, **109**, 21240–21245.

27 W. Zhao, L. Wang, J. Bai, J. S. Francisco and X. C. Zeng, *J. Am. Chem. Soc.*, 2014, **136**, 10661-10668.

28 W. Zhao, J. Bai, L.-F. Yuan, J. Yang, and X. C. Zeng, *Chem. Sci.* 2014, **5**, 1757-1764.

29 W. Zhao, L. Wang, J. Bai, L.-F. Yuan, J. Yang, and X. C. Zeng, *Acc. Chem. Res.,* 2014, **47**, 2505-2513.

30 K. Koga, H. Tanaka and X. C. Zeng, *Nature* 2000, **408**, 564-567.

31 J. Bai, X. C. Zeng, K. Koga and H. Tanaka, *Mol. Simul.* 2003, **29**, 619-626.

32 S. Han, M.Y. Choi, P. Kumar, and H. E. Stanley, *Nat. Phys.* 2010, **6**, 685-689.

33 P. Kumar, S. V. Buldyrev, F. W. Starr, N. Giovambattista, and H. E. Stanley, *Phys. Rev. E* 2005, **72**, 051503.

34 M. W. Mahoney and W. L. Jorgensen, *J. Chem. Phys.* 2000, **112**, 8910-8922.

35 G. A. Kaminski, R. A. Friesner, J. Tirado-Rives and W. L. Jorgensen, *J. Phys. Chem. B* 2001, **105**, 6474-6487.

36 R. C. Rizzo and W. L. Jorgensen, *J. Am. Chem. Soc.* 1999, **121**, 4827–4836.

37 S. Figueroa-Gerstenmaier, S. Giudice, L. Cavallo and G. Milano, *Phys. Chem. Chem. Phys.*, 2009, **11**, 3935–3942.

38 J. G. Harris and K. H. Yung, *J. Phys. Chem.* 1995, **99**, 12021–12024.

39 I. C. Yeh and M. L. Berkowitz, *J. Chem. Phys.* 1999, **111**, 3155.

40 B. Hess, C. Kutzner, D. van der Spoel and E. Lindahl, *J. Chem. Theory Comput.* 2008, **4**, 435-447.

41 S. Nose, *Mol. Phys.,* 1984, **52**, 255-268; W. G. Hoover, *Phys. Rev. A* 1985, **31**, 1695-1697.

42 M. Parrinello and A. Rahman, *J. Appl. Phys.* 1981, **52**, 7182-7190.

43 T. C. W. Mak, *J. Chem. Phys.* 1965, **43**, 2799–2805.

44 K. Koga and H. Tanaka, *J. Chem. Phys.* 1996, **104**, 263–272.

45 S. Alavi, R. Susilo, J. A. Ripmeester, *J. Chem. Phys.* 2009,**130**, 174501.

46 V. Buch, J. P. Devlin, I. A. Monreal, B. Jagoda-Cwikilik, N. Uras-Aytemiz and L. Cwiklik, *Phys. Chem. Chem. Phys.* 2009, **11**, 10245–10265.

47 K. Shin, R. Kumar, K. A. Udachin, S. Alavi and J. A. Ripmeester, *Proc. Natl. Acad. Sci. U.S.A.* 2012, **109**, 14785-14790.

48 R. Zangi and A. E. Mark, *J. Chem. Phys.,* 2003, **119**, 1694-1700.

49 J. S. Loveday, R. J. Nelmes, M. Guthrie, D. D. Klug and J. S. Tse, *Phys. Rev. Lett.* 2001, **87**, 215501.

50 A. Y. Manakov, A. G. Ogienko, M. Tkacz, J. Lipkowski, A. S. Stoporev and N. V. Kutaev, *J. Phys. Chem. B* 2011, **115**, 9564–9569.

51 C. J. Fennell and J. D. Gezelter, *J. Chem. Phys.* 2004, **120**, 9175-9184; *J. Chem. Theory Comput.* 2005, **1**, 662-667.

Graphic Abstract

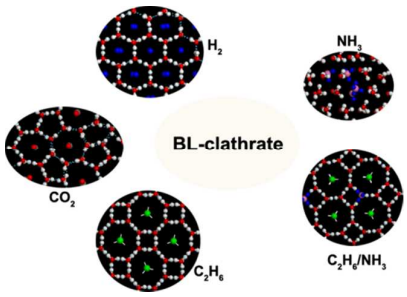

A number of stable BL crystalline and amorphous gas hydrates with either hydrophobic or hydrophilic guest molecules can be formed within a nanoslit